IPPP/06/85
DCPT/06/170
FERMILAB-PUB-07-021-E
Roma-TH-1443

A low energy neutrino factory for large θ_{13}

Steve Geer[1] Olga Mena[2,3] and Silvia Pascoli[4]
[2] *Theoretical Physics Department, Fermi National Accelerator Laboratory, Batavia, IL 60510-0500, USA*
[3] *INFN - Sez. di Roma, Dipartimento di Fisica, Universitá di Roma "La Sapienza", P.le A. Moro, 5, I-00185 Roma, Italy*
[4] *IPPP, Department of Physics, Durham University, Durham DH1 3LE, United Kingdom*
omena@fnal.gov, silvia.pascoli@durham.ac.uk

If the value of θ_{13} is within the reach of the upcoming generation of long-baseline experiments, T2K and NOνA, we show that a low-energy neutrino factory, with peak energy in the few GeV range, would provide a sensitive tool to explore CP-violation and the neutrino mass hierarchy. We consider baselines with typical length 1000–1500 km. The unique performance of the low energy neutrino factory is due to the rich neutrino oscillation pattern at energies between 1 and 4 GeV at baselines $\mathcal{O}(1000)$ km. We perform both a semi-analytical study of the sensitivities and a numerical analysis to explore how well this setup can measure θ_{13}, CP-violation, and determine the type of mass hierarchy and the θ_{23} quadrant. A *low energy neutrino factory* provides a powerful tool to resolve ambiguities and make precise parameter determinations, for both large and fairly small values of the mixing parameter θ_{13}.

PACS numbers: 14.60.Pq

I. INTRODUCTION

During the last several years our understanding of the physics of neutrinos has made remarkable progress. The experiments with solar [1, 2, 3, 4, 5, 6], atmospheric [7], reactor [8], and also long-baseline accelerator [9] neutrinos have provided compelling evidence for the existence of neutrino oscillations, implying non zero neutrino masses. The present data[1] require two large (θ_{12} and θ_{23}) and one small (θ_{13}) angles in the lepton mixing matrix [12], and at least two mass squared differences, $\Delta m^2_{ji} \equiv m^2_j - m^2_i$ (where m_j's are the neutrino masses), one driving the atmospheric (Δm^2_{31}) and the other one the solar (Δm^2_{21}) neutrino oscillations. The mixing angles θ_{12} and θ_{23} control the solar and the dominant atmospheric neutrino oscillations, while θ_{13} is the angle constrained by the data from the CHOOZ and Palo Verde reactor experiments [13, 14].

The Super-Kamiokande [7] and K2K [9] data are well described in terms of dominant $\nu_\mu \to \nu_\tau$ ($\bar\nu_\mu \to \bar\nu_\tau$) vacuum oscillations. The MINOS Collaboration [15] has recently reported the first neutrino oscillation results from 1.27×10^{20} [16]. The value of the oscillation parameters from MINOS are consistent with the ones from K2K, as well as from SK data. A recent global fit [17] (see also Ref. [18]) provides the following 3σ allowed ranges for the atmospheric mixing parameters

$$|\Delta m^2_{31}| = (1.9 - 3.2) \times 10^{-3}\ \text{eV}^2, \quad 0.34 < \sin^2\theta_{23} < 0.68\ . \tag{1.1}$$

The sign of Δm^2_{31}, sign(Δm^2_{31}), cannot be determined with the existing data. The two possibilities, $\Delta m^2_{31} > 0$ or $\Delta m^2_{31} < 0$, correspond to two different types of neutrino mass ordering: normal hierarchy and inverted hierarchy. In addition, information on the octant in which θ_{23} lies, if $\sin^2 2\theta_{23} \neq 1$, is beyond the reach of present experiments.

The 2-neutrino oscillation analysis of the solar neutrino data, including the results from the complete salt phase of the Sudbury Neutrino Observatory (SNO) experiment [6], in combination with the KamLAND spectrum data [19], shows that the solar neutrino oscillation parameters lie in the low-LMA (Large Mixing Angle) region, with best fit values [17] $\Delta m^2_{21} = 7.9 \times 10^{-5}$ eV^2 and $\sin^2\theta_{12} = 0.30$.

[1] We restrict ourselves to a three-family neutrino analysis. The unconfirmed LSND signal [10] cannot be explained within this context and might require additional light sterile neutrinos or more exotic explanations. The ongoing MiniBooNE experiment [11] is going to test the oscillation explanation of the LSND result.

A combined 3-neutrino oscillation analysis of the solar, atmospheric, reactor and long-baseline neutrino data [17] constrains the third mixing angle to be $\sin^2\theta_{13} < 0.041$ at the 3σ C.L. However, the bound on $\sin^2\theta_{13}$ is dependent on the precise value of $|\Delta m^2_{31}|$, being stronger for larger values of $|\Delta m^2_{31}|$. The future goals for the study of neutrino properties in neutrino oscillation experiments is to precisely determine the already measured oscillation parameters and to obtain information on the unknown ones: namely θ_{13}, the CP–violating phase δ and the type of neutrino mass hierarchy (or equivalently sign(Δm^2_{31})).

In the next sections we will explore in detail the possible measurement of the two unknown parameters θ_{13} and δ with a future *neutrino factory* [20] facility as this appears to be among the most promising ways to unveil neutrino mixing and leptonic CP violation [21, 22, 23, 24, 25, 26, 27, 28, 29, 30, 31, 32, 33, 34, 35][2].

A neutrino factory consists of a high intensity muon source[3], an acceleration system, and a muon storage ring with long straight sections. Muons decaying along the straight sections create high intensity neutrino beams which have a precisely-known flux, divergence, energy spectrum, and neutrino flavor content. The flavor composition of the beam depends on whether positive or negative muons are stored in the ring. Suppose, for example, that positive charged muons have been stored. Muons decaying in the straight sections will produce beams containing 50% muon-antineutrinos and 50% electron-neutrinos: $\mu^+ \to e^+ + \nu_e + \bar{\nu}_\mu$. Charged current interactions of the $\bar{\nu}_\mu$ in a distant detector will produce μ^+ ("right-sign" muons, i.e. muons of the same charge as those stored in the neutrino factory). In contrast, if the ν_e's oscillate to ν_μ's and then interact in the far detector they will produce μ^- ("wrong-sign muons" [20, 21]). Thus, wrong-sign muons are an unambiguous proof of electron neutrino oscillation, in the $\nu_e \to \nu_\mu$ channel. This has been called the "golden channel" [26], and is central to the present study. A magnetized detector with excellent charge identification is necessary to exploit the golden channel.

In the following we will consider a *low energy neutrino factory* where the stored muons have an energy of 4.12 GeV. This is motivated by recent progress in developing a viable concept for a neutrino factory detector with a threshold for reliably measuring the sign of muons with momenta down to a few hundred MeV/c [48]. We explore the impact of analyzing the "wrong-sign" and "right-sign" muon rates for several energy bins, and consider two reference baselines: 1280 Km, the distance from Fermilab to Homestake, and 1480 Km, the distance from Fermilab to Henderson mine. Our results can be easily generalized to other baselines in the 1200–1500 km range. We find that a simultaneous fit to the energy-dependent rates provides a powerful tool to resolve ambiguities and make precise parameter determinations, for both large and fairly small values of the mixing parameter θ_{13}.

II. FORMALISM

In the present study we focus on the capabilities of a low-energy neutrino factory, if the value of θ_{13} is within reach of the upcoming generation of long-baseline experiments, T2K and NOνA.

For neutrino energies $E \gtrsim 1$ GeV, θ_{13} within the present bounds [17, 18], and baselines $L \lesssim \mathcal{O}(1000)$ km [51], the oscillation probability $\overset{(-)}{P}(L)$ can be expanded in the small parameters θ_{13}, Δ_{12}/Δ_{13}, Δ_{12}/A and $\Delta_{12}L$, where $\Delta_{12} \equiv \Delta m^2_{21}/(2E)$ and $\Delta_{13} \equiv \Delta m^2_{31}/(2E)$ [26] (see also Ref. [70]):

$$\begin{aligned}\overset{(-)}{P}(L) \simeq\ & \sin^2\theta_{23}\,\sin^2 2\theta_{13}\left(\tfrac{\Delta_{13}}{A\mp\Delta_{13}}\right)^2\sin^2\left(\tfrac{(A\mp\Delta_{13})L}{2}\right)\\ & +\cos\theta_{13}\sin 2\theta_{13}\sin 2\theta_{23}\sin 2\theta_{12}\ \tfrac{\Delta_{12}}{A}\tfrac{\Delta_{13}}{A\mp\Delta_{13}}\ \sin\left(\tfrac{AL}{2}\right)\sin\left(\tfrac{(A\mp\Delta_{13})L}{2}\right)\cos\left(\tfrac{\Delta_{13}L}{2}\mp\delta\right)\\ & +\cos^2\theta_{23}\sin^2 2\theta_{12}\left(\tfrac{\Delta_{12}}{A}\right)^2\sin^2\left(\tfrac{AL}{2}\right)\ ,\end{aligned} \tag{2.1}$$

where the first, second and third terms have been dubbed *atmospheric, interference and solar terms*, respectively. In the following analytical study, we use the constant density approximation for the index of refraction in matter $A \equiv \sqrt{2}G_F\bar{n}_e(L)$. Here, $\bar{n}_e(L) = 1/L\int_0^L n_e(L')dL'$ is the average electron number density, with $n_e(L)$ the electron number density along the baseline.

In order to study the sensitivity to CP-violation, we introduce the weighted probability difference between the case

---

[2] For the prospects of future measurements of these two oscillation parameters at β beam experiments [36, 37], see Refs. [38, 39, 40, 41, 42, 43].

[3] A neutrino factory muon source is an attractive stepping-stone towards a high energy muon collider.

of $\delta \neq 0$ and the one with no CP-violation ($\delta = 0$)[4]:

$$\mathcal{S}(\delta) \equiv \frac{\Big(P(L,\delta) - P(L,0)\Big)^2}{P(L,\delta)} \ , \tag{2.2}$$

$$\bar{\mathcal{S}}(\delta) \equiv \frac{\Big(\bar{P}(L,\delta) - \bar{P}(L,0)\Big)^2}{\bar{P}(L,\delta)} \ . \tag{2.3}$$

The quantity $\mathcal{S}(\delta)$ ($\bar{\mathcal{S}}(\delta)$) is useful to get an estimate of the energy range, for a fixed baseline, for which the sensitivity is maximal. Using Eq. (2.1), we find that:

$$\mathcal{S}(\delta)(\bar{\mathcal{S}}(\delta)) = \frac{4\cos^2\theta_{13}\sin^2 2\theta_{12}\cos^2\theta_{23}\Big(\frac{\Delta_{12}}{\Delta_{13}}\Big)^2\Big(\frac{\Delta_{13}L}{2}\Big)^2\Big(\cos(\delta - \frac{\Delta_{13}L}{2}) - \cos\frac{\Delta_{13}L}{2}\Big)^2}{1 + 2\epsilon\cos(\delta - \frac{\Delta_{13}L}{2}) + \epsilon^2} \tag{2.4}$$

where we have approximated $\cos\theta_{13} \simeq 1$. The quantity ϵ is defined as:

$$\epsilon \equiv \frac{\cos\theta_{23}}{\sin\theta_{23}}\frac{\sin 2\theta_{12}}{\sin 2\theta_{13}}\frac{\Delta_{12}}{\Delta_{13}}\frac{\Delta_{13}L}{2}\frac{A \mp \Delta_{13}}{\Delta_{13}}\frac{1}{\sin((A \mp \Delta_{13})L/2)}, \tag{2.5}$$

where $\mp$ refers to neutrinos (antineutrinos) respectively. At leading order we can neglect A/Δ_{13} terms and ϵ is the same for neutrinos and antineutrinos.

The sensitivity to CP-violation is 0 when the interference term in the oscillation probability, e.g. the second term in the r.h.s. of Eq. (2.1), cancels. For the values of θ_{13} of interest, this happens at the oscillation minima:

$$(\Delta_{13} \mp A)L/2 = n\pi \quad n = 1, 2, 3... \ . \tag{2.6}$$

Neglecting the small correction due to matter effects, we find that the minima in the sensitivity to CP-violation corresponds to an energy of $E_m = 1.4$ (1.2) GeV for L=1480 (1280) km, with $n = 1$. Here and in the following, we used $\Delta m^2_{31} = 2.4 \times 10^{-3}$ eV^2. Matter effects modify this result by 10–20 %. At smaller energies additional minima and maxima with a fast oscillatory behaviour are present but we will not consider such energy range due to detector resolutions, efficiencies and thresholds. As at high energies $\mathcal{S}(\delta)$ and $\bar{\mathcal{S}}(\delta)$ drop as E^{-2}, we expect a maximum in sensitivity at an energy of few GeV. In the case of neutrinos and normal hierarchy (and, for negligible A/Δ_{13}, antineutrinos and inverted hierarchy), an additional minimum in CP-violation sensitivity is found for $\cos(\delta - \Delta_{13}L/2) = \cos(\Delta_{13}L/2)$. This equation has a solution for:

$$\frac{\Delta_{13}L}{2} = \frac{\delta}{2} \qquad \text{for} \quad \delta \geq 0, \tag{2.7}$$

$$\frac{\Delta_{13}L}{2} = \pi - \frac{\delta}{2} \qquad \text{for} \quad \delta < 0. \tag{2.8}$$

For $\delta = \pi/2$ ($-\pi/2$), the energy of the minimum in sensitivity is at $E_m = 5.7$ (1.9) GeV for $L = 1480$ km and at $E_m = 5.0$ (1.7) GeV at $L = 1280$ km. Let us notice that, if $\delta < 0$, the two minima in Eqs. (2.6) and (2.8) are very close and the maximum in between cannot be fully exploited due to limited energy resolution. The maximum in sensitivity at higher energy is located close to the minimum in Eq. (2.6), that is in the energy range $E_M \sim$ (2–3) GeV, depending on the value of δ. For non-negative values of δ, it is possible to make full use of the maximum in sensitivity between the two minima in Eqs. (2.6) and (2.8). Again, the maximal sensitivity will be achieved at E_M of few GeV. In both cases, we can obtain a more precise estimate for E_M by neglecting ϵ and solving the equation $\Big(\cos(\delta - \frac{\Delta_{13}L}{2}) - \cos\frac{\Delta_{13}L}{2}\Big) + \frac{\Delta_{13}L}{2}\Big(\sin(\delta - \frac{\Delta_{13}L}{2}) + \sin\frac{\Delta_{13}L}{2}\Big) = 0$. Notice that this equation holds only far away from the minima. Typically, the maximum is reached in the energy range (1.6–5.2) GeV [(1.4–4.5) GeV] for $L = 1480$ km [$L = 1280$ km]. In particular, for $\delta = \pi/2$ ($-\pi/2$) we have $E_M \simeq 1.7$ (3.2) GeV [1.5 (2.6) GeV] with $L = 1480$ km [$L = 1280$ km]. Matter effects included in ϵ in the denominator modify these results by a 10–20 %.

---

[4] A similar analysis with similar results could be carried out for the case $\delta = \pi$. We present here the analytical study assuming that δ is within the interval $[-\pi/2, \pi/2]$. Our numerical simulations will consider the full δ range $[-\pi, \pi]$.

For neutrinos and inverted hierarchy, (and antineutrinos and normal hierarchy, neglecting terms of order A/Δ_{13}), we find a similar behaviour. The minimum in addition to the one in Eq. (2.6) is reached when $\cos(\delta + \Delta_{13}L/2) = \cos(\Delta_{13}L/2)$ whose solutions are:

$$\frac{\Delta_{13}L}{2} = \pi - \frac{\delta}{2} \qquad \text{for} \quad \delta \geq 0, \tag{2.9}$$

$$\frac{\Delta_{13}L}{2} = \frac{\delta}{2} \qquad \text{for} \quad \delta < 0. \tag{2.10}$$

We can also estimate the position of the maximum by solving the equation $\left(\cos(\delta + \frac{\Delta_{13}L}{2}) - \cos\frac{\Delta_{13}L}{2}\right) - \frac{\Delta_{13}L}{2}\left(\sin(\delta + \frac{\Delta_{13}L}{2}) - \sin\frac{\Delta_{13}L}{2}\right) = 0$. The maximum is reached at approximately the same energy as for neutrinos but with opposite δ. As far as ϵ is negligible, the sensitivity does not depend on θ_{13}. Our approximated analytical results on the energy maxima hold for $\sin^2\theta_{13} \gg 10^{-3}\,(\Delta_{13}L/2)/\sin(\Delta_{13}L/2)$. In conclusion, our analytical study suggests that maximal sensitivity to CP-violation is reached in the few GeV range. Notice that, given one type of hierarchy, neutrinos and antineutrinos have similar behaviour but for opposite values of δ. The combination of the two channels allows to reach optimal sensitivity independently of the true value of the CP-violating phase.

Similar considerations hold also for the sensitivity to the type of hierarchy. We can study a similar quantity: $(P_+ - P_-)^2/P_+$ for neutrinos and antineutrinos. We find that the dominant term is proportional to AL while CP-violating terms constitute a correction at most of 20%–30% for the highest allowed values of $\sin^2 2\theta_{13}$. A minimum in the sensitivity is found in correspondence to the minima of the oscillation probability as in the case of CP-violation studied above. The sensitivity to the type of hierarchy depends on the value of the δ phase once the CP-violating corrections are taken into account. For $0 \leq \delta < \pi/2$, the energy for which a maximum in sensitivity is obtained, E_M, will be an decreasing function of the θ_{13} mixing angle. For example, for $\delta = 0$, the maximum in sensitivity will be reached in the 3.7–2.3 GeV range for $\sin^2\theta_{13} = 0.01$–0.1. Conversely, for $\pi/2 < \delta \leq \pi$, E_M will increase with θ_{13} but typically remain in the 1.3–1.6 GeV range. We can conclude that maximal sensitivity is reached for energies around 1.3–4 GeV. For antineutrinos, a similar behaviour can be found, with the exchange of δ in $\pi - \delta$.

In order to study the sensitivity to CP-violation and type of hierarchy, by exploiting the number of events in a simulated experiment, the energy dependence of the cross sections and fluxes should be included. We can expect the value of the energy for which the maxima of sensitivity are reached to be shifted slightly at higher values.

From the above considerations, we can conclude that the use of a detector with a low threshold and good energy resolution and efficiency at $E \gtrsim 1$ GeV is crucial for exploiting the potentiality of a neutrino factory with baselines in the 1000-1500 Km. In addition, a high energy neutrino beam is not necessary and it is sufficient to use lower energies with respect to the commonly studied options for a neutrino factory with muon energies of 20 or 50 GeV.

III. THE LOW ENERGY NEUTRINO FACTORY CONCEPT

A Neutrino Factory consists of (i) an intense low energy muon source, (ii) a muon beam manipulation and cooling system to maximize the number of muons within a useful acceptance, (iii) a "pre-accelerator" to accelerate the muons from low kinetic energies (typically 100-200 MeV) to about 1 GeV, (iv) a system of one or more accelerators to further accelerate the muons to the desired final energy, and (v) a muon storage ring with long straight sections. Design studies [44, 45, 46] have shown that, for a 20 GeV Neutrino Factory, the 1-20 GeV acceleration systems are expected to account for about 26% of the estimated cost. Hence, if the physics goals can be met using muons with energies much lower than 20 GeV, there is a significant cost advantage. In the following, we first discuss the performance of the far detector (which places a lower limit on the desired Neutrino Factory muon energy), and then discuss the low energy Neutrino Factory and its performance. The primary neutrino oscillation channel at a Neutrino Factory requires identification of wrong-sign muons, and hence a detector with excellent muon charge identification. To obtain the required event rates, the far detector fiducial mass needs to be at least O(10 Kt), and therefore we require a very large magnetized detector. Early studies [32] based on a MINOS-like segmented magnetized detector suggested that, to reduce the charge mis-identification rate to the 10^{-4} level while retaining a reasonable muon reconstruction efficiency, the detected muon needs to have a minimum momentum of 5 GeV. The analysis obtained a 50% reconstruction efficiency for CC neutrino interactions exceeding $\sim$ 20 GeV. This effectively places a lower limit of about 20 GeV on the desired energy of the muons stored in the Neutrino Factory. However, a more recent analysis [48] has shown that, with more sophisticated selection criteria, high efficiencies ($> 80\%$) can be obtained for neutrino interactions exceeding $\sim$ 10 GeV, with efficiencies dropping to $\sim 50\%$ by 5 GeV. The new analysis suggests a MINOS-like detector could be used at a Neutrino Factory with energy less than 20 GeV, but probably not less than 10 GeV. If we wish to consider lower energy Neutrino Factories, we will need a finer grained detector that enables

Turn Number	1	2	3	4	5
Initial Energy (GeV)	1.0	1.96	2.92	3.88	4.84
Final Energy (GeV)	1.48	2.44	3.40	4.36	5.32
$f_{decay} = 100m/\gamma c\tau$ (%)	1.30	0.73	0.51	0.39	0.32
N_{decay} per year ($\times 10^{18}$)	9.8	5.5	3.8	2.9	2.4

TABLE I: *Useful positive muon decays in one straight section of an RLA designed to accelerate from 1 GeV to 5.8 GeV in 5 turns. The straight section and arc lengths are, respectively, 100m and 30m. The numbers tabulated correspond to* 7.5×10^{20} *injected muons, or roughly one years operation.*

reliable sign-determination of lower energy muons with good efficiency. One way to achieve this would be to use a totally active magnetized segmented detector, for example a NOvA-like detector [47] within a large magnetic volume. Initial studies [48] show that, for this technology, the muon reconstruction efficiency is expected to approach unity for momenta exceeding $\sim$ 200 MeV/c, with a charge mis-identification lower than 10^{-4} (10^{-3}) for momenta exceeding approximately 400 MeV/c (300 MeV/c).

Further studies are needed to fully understand the efficiency and mis-identification as a function of neutrino energy, but there is hope that a Neutrino Factory detector might be designed with good wrong-sign muon identification and high efficiency for neutrino energies as low as 1 GeV, or perhaps a little lower. Given these recent developments, in our analysis we will assume that a massive magnetized detector can be designed to identify wrong-sign muons with full efficiency for neutrino interactions above 0.8 GeV, and zero efficiency below this energy. We will see that the excellent physics capability of a low energy Neutrino Factory motivates striving for a detector that can achieve this demanding performance.

With a magnetized far detector concept that makes plausible precision measurements of neutrino interactions down to about 0.8 GeV, we are motivated to consider Neutrino Factories with stored muon energies of a few GeV. In present designs for a 20 GeV Neutrino Factory [46], there are at least two acceleration stages that accelerate the muons from about 1 GeV to 20 GeV. Depending on the design, these accelerators consist either of Recirculating Linear Accelerators (RLAs) or Fixed Field Alternating Gradient accelerators (FFAGs). A few GeV Neutrino Factory would require only one of these acceleration stages. Note that the RLAs have long straight acceleration sections which, if pointing in a suitable direction, could provide a neutrino beam with a time-dependent energy that varies from 200 MeV up to the final energy. This might facilitate a tunable-energy Neutrino Factory. To illustrate this, Table I shows, for 7.5×10^{20} positive muons (per year) injected into an 1-5.8 GeV RLA, the number of muon decays in a given straight section at each intermediate energy. Only 7% of the injected muons decay during the acceleration, and hence 93% (7×10^{20}) are available to be injected into a dedicated fixed-energy Neutrino Factory. If the Neutrino Factory straight section length is 30% of the ring circumference, this would provide an additional 2×10^{20} useful muon decays per year at 5.8 GeV. Note that using the RLA to provide a neutrino beam would provide flexibility in choosing the desired neutrino energy spectrum. The acceleration cycle could, in principle, be varied to keep the muons for as long as desired at any intermediate energy. Hence, the 2×10^{20} useful muon decays could be redistributed amongst the intermediate energies, as needed. However, the flexibility of using the RLA to provide a low energy neutrino beam comes at the cost of a more complicated design for the accelerator. In particular, the angular divergence of the beam within the straight section needs to be small compared to the angular spread of the neutrinos generated in muon decay. If designs that achieve this prove to be impractical or expensive, flexibility could also be achieved by designing the RLA so that the muons could be extracted on any given turn and injected into one of several fixed energy Neutrino Factory storage rings (note that the cost of the storage rings is believed to be small compared to the cost of the RLA).

In the following we will show that a low energy Neutrino Factory with a fixed energy of 4.12 GeV would provide a sensitive tool for exploring neutrino oscillations if θ_{13} is "large". This energy would require about 4 turns in a single RLA. Note that the sensitivity of a Neutrino Factory experiment depends upon the event statistics, and hence upon the product of the detector fiducial mass, the length of the data taking period, and the number of muons per unit time decaying in the appropriate Neutrino Factory straight section. Initial studies have considered, as reasonable, a totally active magnetized detector with a fiducial mass of about 20 Kt. Present Neutrino Factory studies suggest that it would be reasonable to expect, for a Neutrino Factory with (without) a muon cooling channel before the pre-accelerator, about 5×10^{20} (3×10^{20}) useful positive muon decays per year and 5×10^{20} (3×10^{20}) useful negative muon decays per year in a given Neutrino Factory straight section. Hence, a conservative estimate of the sensitivity of a Neutrino Factory experiment might be based upon 5 years data taking with 3×10^{20} useful muon decays of each sign per year in the storage ring, and a detector fiducial mass of 20 Kt, corresponding to 3×10^{22} Kt-decays for each muon sign. A more aggressive estimate might be based upon 10 years data taking with 5×10^{20} useful muon decays of each sign per year in the storage ring, and a detector fiducial mass of 20 Kt, corresponding to 1×10^{23} Kt-decays

for each muon sign.

IV. NUMERICAL ANALYSIS: DEGENERATE SOLUTIONS

We can ask ourselves whether it is possible to unambiguously determine δ and θ_{13} by measuring the transition probabilities $\nu_e \to \nu_\mu$ and $\bar{\nu}_e \to \bar{\nu}_\mu$ at fixed neutrino energy and at just one neutrino factory baseline. The answer is no. It has been shown [29] that, by exploring the full (allowed) range of the δ and θ_{13} parameters, that is, $-180^\circ < \delta < 180^\circ$ and $0^\circ < \theta_{13} < 10^\circ$, one finds, at fixed neutrino energy and at fixed baseline, the existence of degenerate solutions $(\theta_{13}^{'},\ \delta^{'})$, that have been labelled in the literature *intrinsic degeneracies*, which give the same oscillation probabilities as the set $(\theta_{13},\ \delta)$ chosen by nature. More explicitly, if $(\theta_{13},\ \delta)$ are the correct values, the conditions

$$P_{\nu_e\nu_\mu}(\theta_{13}^{'},\delta^{'}) = P_{\nu_e\nu_\mu}(\theta_{13},\delta)$$
$$P_{\bar{\nu}_e\bar{\nu}_\mu}(\theta_{13}^{'},\delta^{'}) = P_{\bar{\nu}_e\bar{\nu}_\mu}(\theta_{13},\delta)$$

can be generically satisfied by another set $(\theta_{13}^{'},\ \delta^{'})$.

Additional solutions might appear from unresolved degeneracies in two other oscillation parameters:

1. At the time of the future neutrino factory, the sign of the atmospheric mass difference Δm^2_{31} may remain unknown, that is, we would not know if the hierarchy of the neutrino mass spectrum is normal or inverted. In this particular case, $P(\theta_{13}^{'},\delta^{'},-\Delta m^2_{31}) = P(\theta_{13},\delta,\Delta m^2_{31})$.

2. Disappearance experiments only give us information on $\sin^2 2\theta_{23}$: is θ_{23} in the first octant, or is it in the second one, $(\pi/2-\theta_{23})$? . In terms of the probabilities, $P(\theta_{13}^{'},\delta^{'},\frac{\pi}{2}-\theta_{23}) = P(\theta_{13},\delta,\theta_{23})$.

This problem is known as the problem of degeneracies in the neutrino parameter space [29, 30, 49, 50, 51, 52]. All these ambiguities complicate the experimental determination of δ and θ_{13}. Many strategies have been advocated to resolve this issue which in general involve another detector [29, 31, 53, 54, 55, 56, 57, 58] or the combination with another experiment [34, 35, 59, 60, 61, 62, 63, 64, 65, 66, 67].

In the present study we show that, if the value of θ_{13} turns out to be not very small, a *low energy neutrino factory* provides the ideal scenario for the extraction of the unknown parameters as well as for resolving the discrete degeneracies. The reason is simple: at distances of $\mathcal{O}(1000)$ km the neutrino oscillation pattern is extremely rich at neutrino energies below 4 GeV. We have thus explored a single decaying muon energy scenario $E_\mu = 4.12$ GeV.

By exploiting the energy dependence of the signal, it is possible to disentangle θ_{13} and δ and to eliminate the additional solutions arising from the discrete ambiguities. We have divided the signal in four energy bins. The energy binning of the signal has been chosen accordingly to the analytical study. The energy range of these four energy bins is $[0, 0.8]$, $[0.8, 1.5]$, $[1.5, 3.5]$ and $[3.5, 4.12]$ GeV. We will show the physics potential of the chosen energy binning here in the next subsection. The detection efficiencies are considered as perfect (100%) above the first bin, as described in the previous section.

Two possible baselines have been carefully explored: 1280 Km, the distance from Fermilab to Homestake, and 1480 Km, the distance from Fermilab to Henderson mine. The results are presented for the two possible scenarios described in the previous section, in order to quantify the benefits of increased exposure times and muon intensities: a conservative scenario of 3×10^{22} Kton-decays and a more ambitious one with 1×10^{23} Kton-decays.

All numerical results simulated in the next subsections here have been obtained with the exact formulae for the oscillation probabilities. Unless specified otherwise, we take the following central values for the remaining oscillation parameters: $\sin^2\theta_{12} = 0.29$, $\Delta m^2_{21} = 8 \times 10^{-5}$ eV^2, $|\Delta m^2_{31}| = 2.5 \times 10^{-3}$ eV^2 and $\theta_{23} = 40^\circ$. The χ^2 for a fixed baseline λ is defined as:

$$\chi^2_\lambda = \sum_{i,j}\sum_{p,p'} (n^\lambda_{i,p} - N^\lambda_{i,p}) C^{-1}_{i,p:,j,p'} (n^\lambda_{j,p'} - N^\lambda_{j,p'})\,, \tag{4.1}$$

where $N^\lambda_{i,\pm}$ is the predicted number of muons for a certain oscillation hypothesis, $n^\lambda_{i,p}$ are the simulated "data" from a Gaussian or Poisson smearing and C is the $2N_{bin} \times 2N_{bin}$ covariance matrix, that will contain statistical errors and a 2% overall systematic error. All the contour plots presented in the following in a two parameter space have been performed assuming 2 d.o.f statistics.

A. Optimizing the energy binning

In this subsection we provide an explanation for the energy binning chosen here, crucial to resolve the additional solutions (degeneracies). As first noticed in Ref. [59], the location of the degeneracies is E, L dependent. For large θ_{13}, the location of the *intrinsic* degeneracies is given by:

$$\begin{aligned} \delta^{'} &\simeq \pi - \delta, \\ \theta_{13}^{'} &\simeq \theta_{13} + \cos\delta \sin 2\theta_{12} \frac{\Delta m^2_{21} L}{4E} \cot\theta_{23} \cot\left(\frac{\Delta m^2_{31} L}{4E}\right) . \end{aligned} \tag{4.2}$$

Notice that the shift $\theta_{13}^{'} - \theta_{13}$ depends on the energy and the baseline through the function $\cot\left(\frac{\Delta m^2_{31} L}{4E}\right)$. If the function $\cot\left(\frac{\Delta m^2_{31} L}{4E}\right)$ changes sign from one energy bin to another, the degenerate solutions will appear in different regions of the parameter space. Consequently, the combination of fits to the various energy bins can eliminate the *intrinsic* degeneracies.

To illustrate this, Figure (1)(a) depicts results from fitting the simulated data for each of the energy bins. The simulation is for $L = 1480$ km, $\theta_{13} = 3°$, $\delta = 0°$, normal mass hierarchy, and $\theta_{23} = 40°$. The fit results shown in the figure correspond to the correct hierarchy and θ_{23} (the impact of including the discrete degeneracies will be discussed later). The 90%, 95% and 99% CL contours resulting from the fits are shown for the second energy bin (blue), third energy bin (cyan,) and fourth energy bin(magenta). Notice that in addition to the correct solution, there are also fake solutions for which $\delta^{'} \simeq \pi$, as indicated by Eq. (4.2). However, the fake solutions from the fit to the third energy bin get opposite displacements $\theta_{13}^{'} - \theta_{13}$ from those from the fits to the second and fourth energy bins. The relative displacement (positive or negative) is given by the sign of the trigonometric function $\cot\left(\frac{\Delta m^2_{31} L}{4\langle E\rangle}\right)$, where $\langle E\rangle$ is the medium energy for a fixed bin. A combination of fits to the second, third and fourth energy bins will therefore help in resolving the *intrinsic* degeneracies.

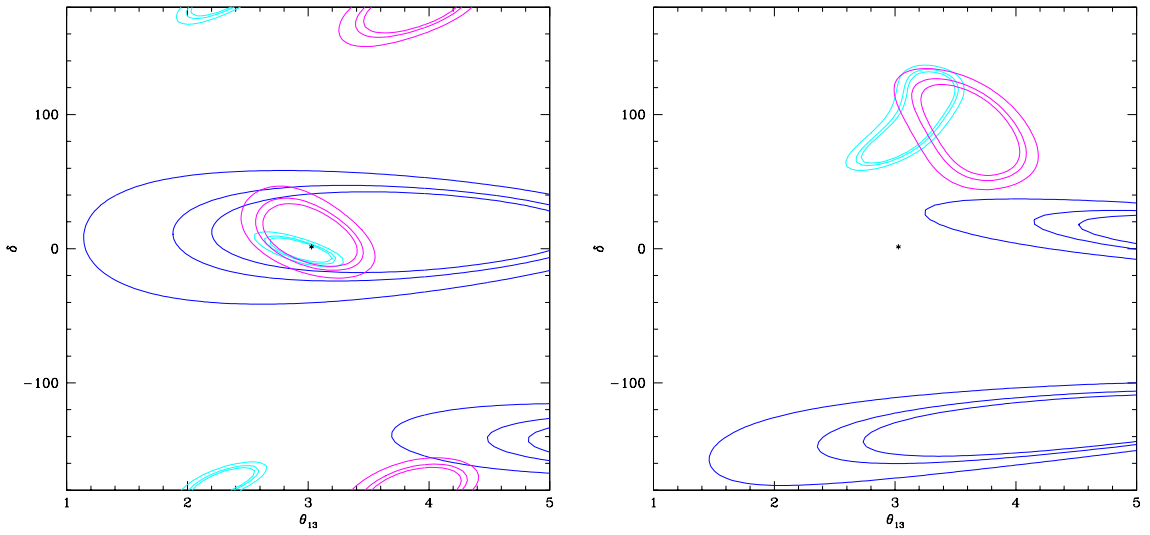

(a) Intrinsic degeneracies

(b) Sign Δm^2_{31} degeneracies

FIG. 1: 90%, 95% *and* 99% *(2 d.o.f) contours resulting from fits to simulated data for* $L = 1480$ *km,* $\theta_{13} = 3°$*, and* $\delta = 0°$ *(position in parameter space denoted by a star). The blue, cyan and magenta contours represent the results from fits to the second, third and fourth energy bins, respectively. In the left panel, we have neglected the impact of the discrete degeneracies. In the right panel, the fit assumes incorrectly that the sign of the atmospheric mass difference is negative. The atmospheric mixing angle is fixed to* $\theta_{23} = 40°$*.*

A similar exercise to the one described above can be done for the discrete degeneracies. For instance, the wrong-sign(Δm^2_{31}) additional solutions will be located in different regions of the parameter space for each energy bin, see Fig. (1)(b), and therefore fits to the combination of the energy bins will result in a resolution of the *sign* degeneracies.

The location of the fake solutions for the second energy bin is different from those for the third and fourth energy bins, since at lower energies matter effects are less important.

Resolving the additional θ_{23}-octant degeneracy is, in general, very difficult. As shown in Ref. [59], for large θ_{13}, the location of the θ_{23} degeneracies is given by:

$$\begin{aligned} \sin\delta^{'} &\simeq \cot\theta_{23}\ \sin\delta, \\ \theta_{13}^{'} &\simeq \tan\theta_{23}\ \theta_{13} + \frac{\sin 2\theta_{12}\frac{\Delta m^2_{21}L}{4E}}{2\sin\left(\frac{\Delta m^2_{31}L}{4E}\right)}\left(\cos\left(\delta - \frac{\Delta m^2_{31}L}{4E}\right) - \tan\theta_{23}\cos\left(\delta^{'} - \frac{\Delta m^2_{31}L}{4E}\right)\right). \end{aligned} \tag{4.3}$$

This system describes two solutions. For one of them, the L and E dependent terms in Eq. (4.3) tend to cancel for $\theta_{23} \to \pi/4$, resulting in $\theta_{13}^{'} = \theta_{13}$ and $\delta^{'} = \delta$ in this limit. The second solution coincides in this limit with the intrinsic degeneracy, Eq. (4.2). Notice that no fake solutions are expected for $|\cot\theta_{23}\ \sin\delta| > 1$. Figure (2) illustrates the equivalent exercise to those performed above for the *intrinsic* and for the wrong-sign(Δm^2_{31}) degeneracies. The simulated data is for the θ_{23} in the first octant, i.e. $\theta_{23} = 40^\circ$, while the fit is performed incorrectly assuming the second octant, i.e. $\theta_{23} = 50^\circ$. Notice from the results depicted in Fig. (2)(a) that there are two sets of degenerate solutions, as previously discussed: those which resemble the correct values and those which are related to the intrinsic solution. While the location of the former is E, L independent, the location of the latter will depend on E, L, and therefore the combined fits to the various energy bins will help in resolving these degeneracies. Note that the degeneracies which are closer to the correct values are extremely difficult to resolve. The information in the second bin is crucial: if the detector efficiency in the second bin ($[0.8, 1.5]$ GeV) is sufficiently high (we are assuming 100%), the combination of fits to the various energy bins will resolve the additional solutions related to the wrong choice of the atmospheric mixing angle octant. Since the second bin is the lower energy bin, it turns out that for these lower energies the solar term, see Eq. (2.1), is the dominant one for $\theta_{13} \leq 3^\circ$, larger than both the atmospheric and the interference terms. The solar term goes as $\cos^2\theta_{23}$, while the atmospheric term goes as $\sin^2\theta_{23}$, therefore, exploiting this low energy bin is crucial to resolve the θ_{23} degeneracy. The resulting fit, after the combination of the data in the three energy bins considered here, is degeneracy free down to very small values of $\theta_{13} \simeq 1^\circ$ (see Fig. (2)(b)), since the additional solutions from fits to the second bin lie on different locations in parameter space than those for the third and fourth energy bins.

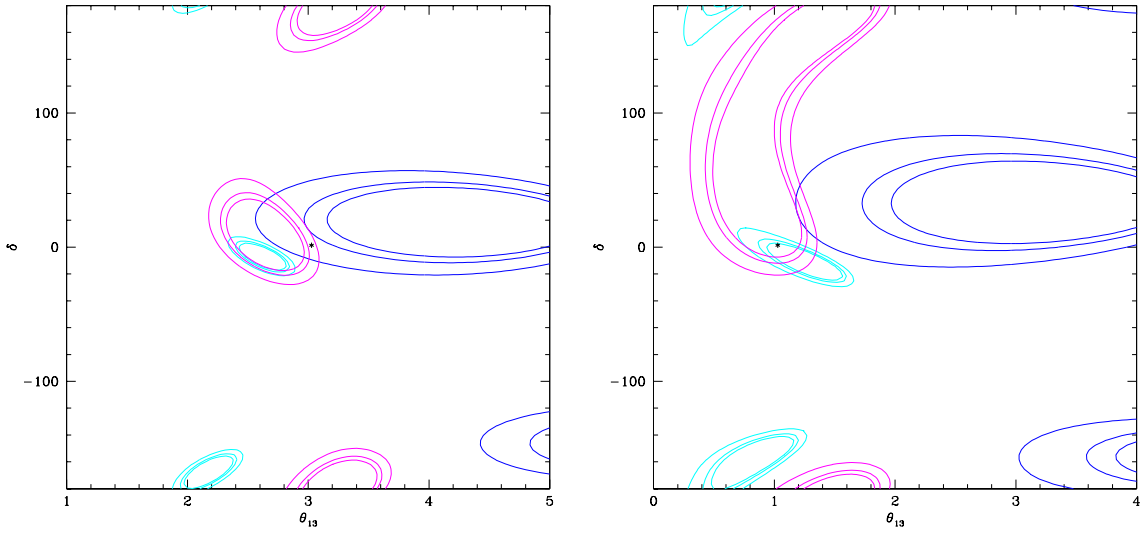

(a) $\theta_{13} = 3^\circ$ (b) $\theta_{13} = 1^\circ$

FIG. 2: *(a)* 90%, 95%*and* 99% *(2 d.o.f) contours resulting from the fits to the data at* $L = 1480$ *km, assuming that the nature solution is* $\theta_{13} = 3^\circ$ *and* $\delta = 0^\circ$ *(denoted by a start). The blue, cyan and magenta contours represent the results with the second, third and fourth energy bin data, respectively. We assume that the true value of the atmospheric mixing angle is* $\theta_{23} = 40^\circ$ *(first octant) but the data is fitted to* $\theta_{23} = 50^\circ$ *(second octant). (b) Same than in (a) but assuming that the nature solution is* $\theta_{13} = 1^\circ$ *and* $\delta = 0^\circ$ *(denoted by a start).*

B. Exploring the disappearance channel

We explore here the measurement of the atmospheric neutrino oscillation parameters, θ_{23} and Δm^2_{31} making use of the ν_μ disappearance channel. We study as well the impact of this channel regarding the θ_{23}-octant degeneracy. The disappearance channel at the neutrino factory has been already considered in the literature [24, 68] and it has been widely and carefully explored in Ref. [69] . The vacuum $\nu_\mu \to \nu_\mu$ oscillation probability expanded to the second order in the small parameters θ_{13} and $(\Delta_{12}L/E)$ reads [70]

$$\begin{aligned} P(\nu_\mu \to \nu_\mu) &= 1 - \left[\sin^2 2\theta_{23} - s^2_{23} \sin^2 2\theta_{13} \cos 2\theta_{23}\right] \sin^2\left(\frac{\Delta_{23}L}{2}\right) \\ &- \left(\frac{\Delta_{12}L}{2}\right) \left[s^2_{12} \sin^2 2\theta_{23} + \tilde{J} s^2_{23} \cos\delta\right] \sin(\Delta_{23}L) \\ &- \left(\frac{\Delta_{12}L}{2}\right)^2 \left[c^4_{23} \sin^2 2\theta_{12} + s^2_{12} \sin^2 2\theta_{23} \cos(\Delta_{23}L)\right] , \end{aligned} \tag{4.4}$$

where $\tilde{J} = \cos\theta_{13} \sin 2\theta_{12} \sin 2\theta_{13} \sin 2\theta_{23}$ and $\Delta_{23} = \Delta m^2_{32}/2E$, $\Delta_{12} = \Delta m^2_{21}/2E$. The first term in the first parenthesis is the dominant one and is symmetric under $\theta_{23} \to \pi/2 - \theta_{23}$. However, when a rather large non-vanishing θ_{13} is switched on, a θ_{23}-asymmetry appears in Eq. (4.4) and the octant in which θ_{23} lies can be extracted from disappearance data, as will be shown in our numerical results. We assume here the same detection efficiencies[5] and energy binning than those which will be considered for the golden $\nu_e \to \nu_\mu$ transition. A global 2% systematic error has been included in the χ^2 fits to the atmospheric neutrino parameters. We present our results in the $(\sin^2\theta_{23}, \Delta m^2_{31})$ plane in Figs. (3) for two simulated values of θ_{13}, and two simulated values for $\sin^2\theta_{23}$: $\sin^2\theta_{23} = 0.4$ and $\sin^2\theta_{23} = 0.44$. The detector is located at the Henderson mine at a baseline of $L = 1480$ km (similar results are obtained for the Homestake detector location). The CP violating phase δ has been set to zero. Notice that this channel is able to reduce atmospheric parameter uncertainties to an unprecedented level: the resolution in $\sin^2\theta_{23}$ is astonishing, maximal mixing can be excluded at 99% CL if $\sin^2\theta_{23} < 0.48$ ($\theta_{23} < 43.8°$), independently of the value of θ_{13}. In addition, for a relatively *large* value of $\theta_{13} > 8°$, the θ_{23}-octant degeneracy will not be present at the 99% CL for $\sin^2\theta_{23} < 0.44$ ($\theta_{23} < 41.5°$), if θ_{13} is treated as a fixed parameter. These results have been obtained for the more conservative neutrino factory scenario described above, a scenario with 3×10^{22} Kton-decays for each muon sign. Since the statistics and the size of the expected signal are both large in disappearance measurements, the error on the parameters will be dominated by the systematic error and a more ambitious scenario with higher statistics (with 1×10^{24} Kton-decays) will not improve much these results.

C. Simultaneous fits to θ_{13} and δ

In this subsection we exploit the *golden channel*, i.e. the $\nu_e(\bar{\nu}_e) \to \nu_\mu(\bar{\nu}_\mu)$ transitions to extract the unknown parameters θ_{13} and δ. We start exploring the more conservative neutrino factory scenario with 3×10^{22} Kton-decays. We present in Figs. (4) the 90%, 95% and 99% CL contours for a fit to the simulated data from a future low energy neutrino factory with the detector located at Homestake, at a baseline $L = 1280$ km (left panel) and at Henderson, at a baseline $L = 1480$ km (right panel). The "true" parameter values that we have chosen for these examples are depicted in the figures with a star: we have explored four different values of $\delta = 0°$, $90°$, $-90°$ and $180°$ and $\theta_{13} = 8°$. The simulations are for the normal mass hierarchy and θ_{23} in the first octant ($\sin^2\theta_{23} = 0.41$ which corresponds to $\theta_{23} = 40°$). Our analysis includes the study of the discrete degeneracies. That is, we have fitted the data assuming both the wrong hierarchy and the wrong choice for the θ_{23} octant (i.e. negative hierarchy and $\sin^2\theta_{23} = 0.59$, which corresponds to $\theta_{23} = 50°$) and the additional solutions (if present) will be shown in red and in cyan, respectively. Notice that in Figs. (4) the sign ambiguity is solved at the 99% CL. The additional solutions associated to the wrong choice of the θ_{23} octant are not present at the same CL due to the information extracted from the disappearance channel.

Similar results are obtained for smaller values of θ_{13}, see Figs. (5). Notice that the performance of the *low energy neutrino factory* is unique: the sign(Δm^2_{31}) can be determined at the 99% if $\theta_{13} > 2°$ independent of the value of the CP phase δ. Regarding the θ_{23}-octant ambiguity, it can be removed at the 99% CL down roughly to $\theta_{13} > 1°$ for a

[5] We believe this is conservative since less aggressive cuts are required to reduce backgrounds for the disappearance channel than those required for the appearance channel.

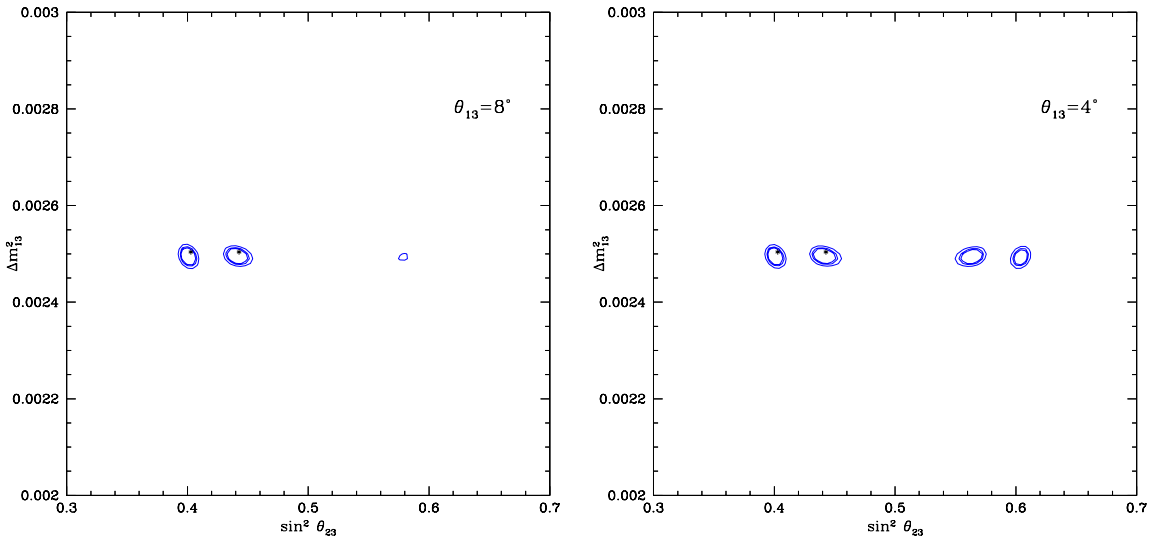

(a) $\theta_{13} = 8^\circ$ (b) $\theta_{13} = 4^\circ$

FIG. 3: 90%, 95% *and* 99% *(2 d.o.f) CL contours resulting from the fits at* $L = 1480$ *km assuming two central values for* $\sin^2\theta_{23} = 0.4$ *and* 0.44 *and* $\Delta m^2_{31} = 2.5 \times 10^{-3}$ eV^2. *In the right (left) panel,* $\theta_{13} = 8^\circ$ (4°). *A larger value of* θ_{13} *introduces a larger asymmetry and the four-fold degeneracy in the atmospheric neutrino parameters is solved. The statistics considered for both simulations corresponds to* 3×10^{22} *Kton-decays. Only disappearance data have been used to perform these plots.*

nature's choice of $\sin^2\theta_{23} = 0.41$, independent of the value of δ, provided that the conservative estimate of 3×10^{22} Kt-decays for each muon sign are feasible. The θ_{23} octant degeneracy is solved with the information contained in the second energy bin data, which is sensitive to the solar term, as mentioned before.

Since the results are very similar for the two baselines explored here, the physics reach with the more aggressive estimate of 1×10^{23} Kt-decays for each muon sign is illustrated for only one baseline, $L = 1480$ km (Henderson mine site) and for smaller values of θ_{13}. Figure (6) shows fit results for two simulated values of θ_{13} (2° and 1°). The mass hierarchy can be determined at the 99% CL if $\theta_{13} > 1^\circ$ independent of the value of the CP phase δ. In addition, for our example with $\sin^2\theta_{23} = 0.41$, the θ_{23} octant ambiguity can be resolved at 99%CL for all values of the CP phase δ provided $\theta_{13} > 0.6^\circ$.

We summarize the reach of the low energy neutrino factory with two exclusion plots which illustrate the performance of the experiment explored here. We have taken into account the impact of both the intrinsic and discrete degeneracies to depict the excluded regions. For both exclusion plots we have assumed that the detector is located at the Henderson mine at $L = 1480$ km. The results for the closer baseline ($L = 1280$ km) are very similar.

Figure (7) depicts the region in the $\sin^2 2\theta_{13}$, fraction of δ plane for which the hierarchy can be resolved at the 95% CL assuming 2 d.o.f statistics, for both scenarios, the more conservative one, in which the exposure is 3×10^{22} Kton-decays, and the more aggressive scenario in which the exposure is 1×10^{23} Kton-decays. Notice that the hierarchy could be determined in both scenarios if $\sin^2 2\theta_{13} > 0.01$ (i.e. $\theta_{13} > 3^\circ$) regardless of the value of the CP violating phase δ.

Figure (8) depicts the region in the ($\sin^2 2\theta_{13}$, δ) plane for which a given (non-zero) value of the CP violating phase can be distinguished at the 95% CL from the CP conserving case, i.e. $\delta = 0, \pm 180^\circ$ (assuming 2 d.o.f statistics). This exercise is illustrated for the two scenarios considered in this study, the more conservative one, in which the exposure is 3×10^{22} Kton-decays, and the more agressive scenario in which the exposure is 1×10^{23} Kton-decays. Notice that the CP violating phase δ could be measured with a 95% CL error lower than 20° in both scenarios if $\sin^2 2\theta_{13} > 0.01$ (i.e. $\theta_{13} > 3^\circ$), reaching an unprecedent precision for larger values of θ_{13}. For smaller values, $0.001 < \sin^2 2\theta_{13} < 0.01$, and in the more conservative scenario, the presence of the sign-degeneracy compromises the extraction of the CP violating phase δ. On the other hand, in the more aggressive scenario, a CP violating effect could be established at the 95% CL if $\sin^2 2\theta_{13} \geq 0.001$ for $20^\circ < \delta < 160^\circ$ $(-160^\circ < \delta < -20^\circ)$.

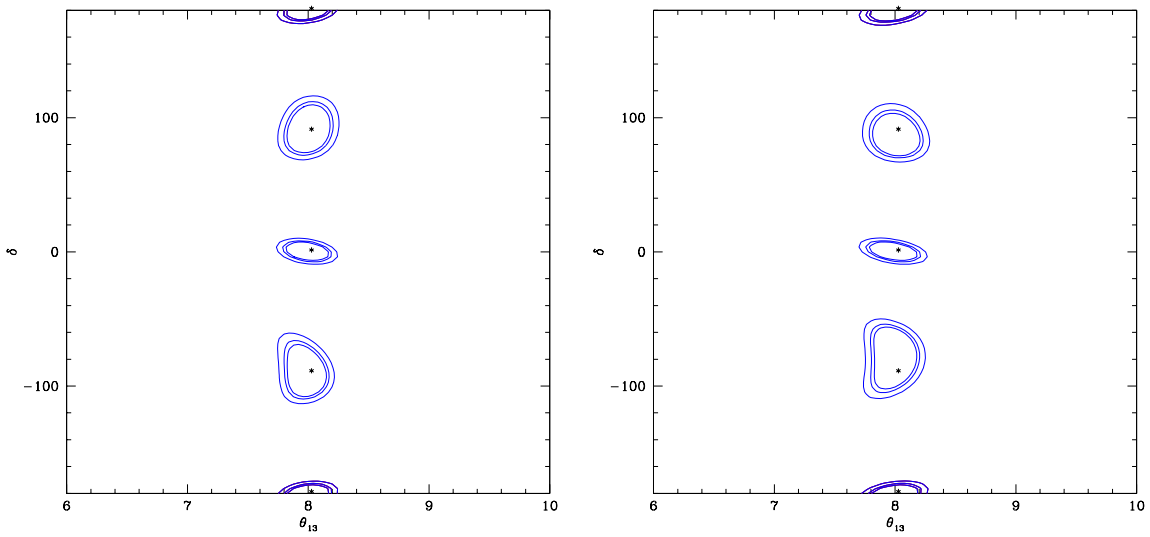

(a) Homestake, $L = 1280$ km. (b) Henderson, $L = 1480$ km

FIG. 4: 90%, 95% *and* 99% *(2 d.o.f) CL contours resulting from the fits at* $L = 1280$ *km (left panel) and* $L = 1480$ *km (right panel) assuming four central values for* $\delta = 0°$, $90°$, $-90°$ *and* $180°$ *and* $\theta_{13} = 8°$. *The statistics considered for both simulations corresponds to* 3×10^{22} *Kton-decays.*

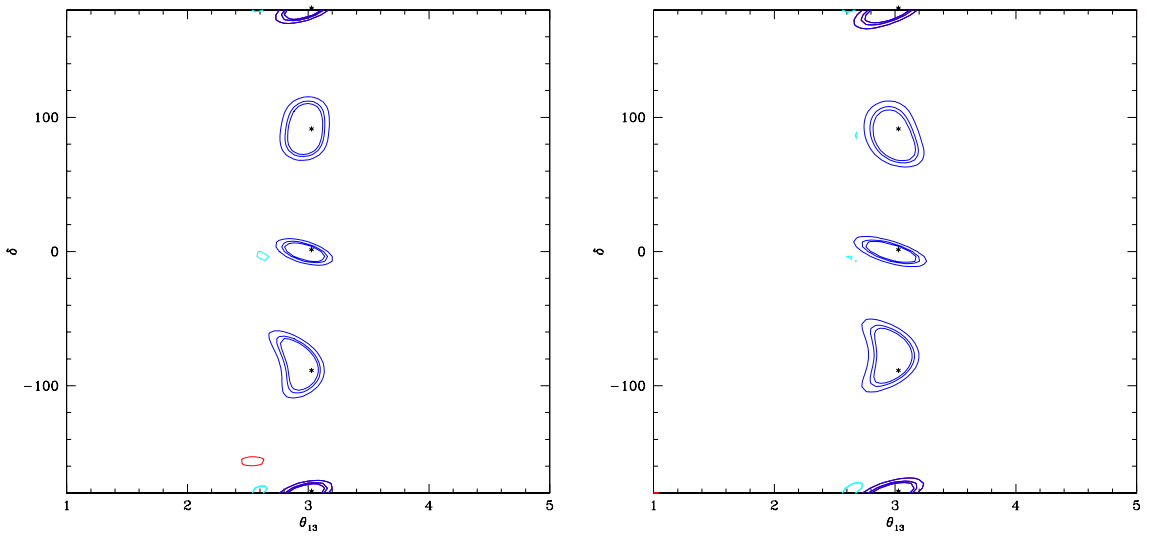

(a) Homestake, $L = 1280$ km. (b) Henderson, $L = 1480$ km

FIG. 5: *The same as Figs. (4) but for* $\theta_{13} = 3°$. *The additional solution (only at the* 99% *CL) associated to the wrong choice of the neutrino mass ordering is depicted in red. The additional solutions (only at the* 99% *CL) arising from the wrong choice of the* θ_{23} *octant are depicted in cyan. The statistics considered for both simulations corresponds to* 3×10^{22} *Kton-decays.*

V. CONCLUSIONS

We have shown here the enormous physics reach of a novel neutrino factory concept, a *low energy neutrino factory*, in which the stored muons have an energy of 4.12 GeV.

We have exploited both the disappearance ($\nu_\mu \to \nu_\mu$) and the *golden* ($\nu_e \to \nu_\mu$) channels by measuring the "right-sign" and the "wrong-sign" muons at a two possible baselines: 1280 Km, the distance from Fermilab to Homestake,

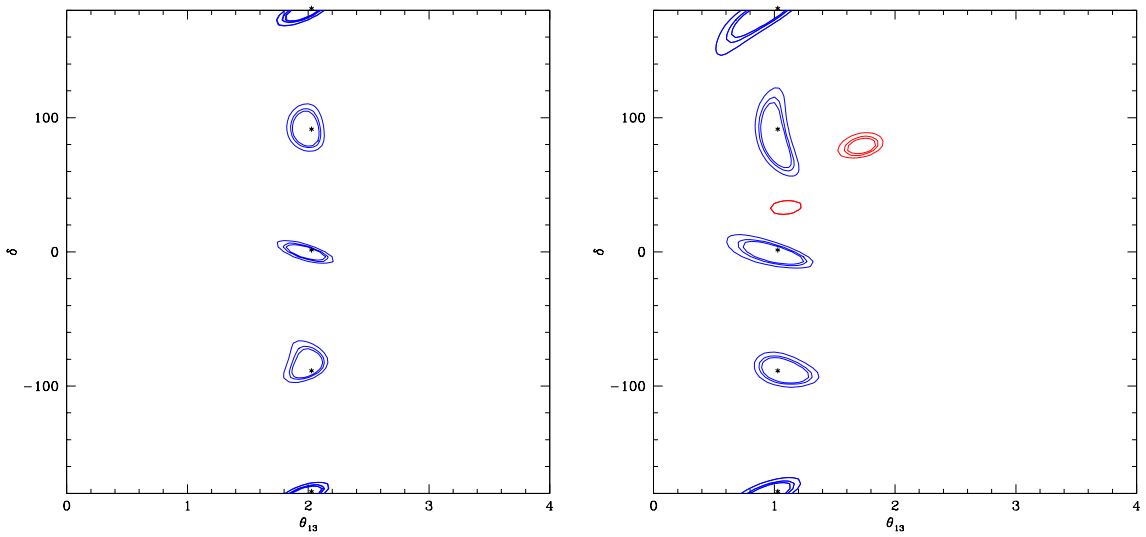

(a) $\theta_{13} = 2^\circ$ (b) $\theta_{13} = 1^\circ$

FIG. 6: 90%, 95% *and* 99% *(2 d.o.f) CL contours resulting from the fits at* $L = 1480$ *km assuming four central values for* $\delta = 0^\circ$, 90°, -90° *and* 180° *and* $\theta_{13} = 2^\circ$ *in the left panel (*$\theta_{13} = 1^\circ$ *in the right panel). The additional solutions associated to the wrong choice of the neutrino mass ordering are depicted in red. The statistics considered for both simulations corresponds to* 1×10^{23} *Kton-decays.*

and 1480 Km, the distance from Fermilab to Henderson mine. The results presented here can be easily generalized to other baselines in the 1200–1500 km range.

We illustrate the results of the analysis of the energy binned signal for a facility with (a) 3×10^{22} Kt-decays for each muon sign and (b) 1×10^{23} Kt-decays for each muon sign. The novel setup presented here could extract the θ_{13} angle, the neutrino mass hierarchy and the leptonic CP violating phase δ with unprecedented precision.

The unique performance of the *low energy neutrino factory* (when compared to the common $20 - 50$ GeV neutrino factory) is due to the rich neutrino oscillation pattern at energies between 1 and 4 GeV at baselines $\mathcal{O}(1000)$ km. Recent studies have shown that it could be possible a Neutrino Factory detector with good wrong-sign muon identification and high efficiency for neutrino energies as low as 1 GeV, or perhaps a little lower. Therefore, to evaluate the physics potential of a low energy neutrino factory, we have assumed 100% efficiency above a threshold energy of 0.8 GeV, and zero efficiency below this threshold. This naïve model for the detector performance will need to be updated once further work has been done to better understand the expected detector energy dependent efficiency.

With this caveat we find that maximal atmospheric neutrino mixing can be excluded at 99% CL if $\sin^2\theta_{23} < 0.48$ ($\theta_{23} < 43.8^\circ$). If the atmospheric mixing angle is not maximal, for a nature's choice of $\sin^2\theta_{23} = 0.4$, the octant in which θ_{23} lies could be extracted at the 99% CL if $\theta_{13} > 1^\circ$ ($\theta_{13} > 0.6^\circ$) with an exposure of 3×10^{22} Kt-decays (1×10^{23} Kt-decays) for each muon sign, independently of the value of the CP violating phase δ. The neutrino mass hierarchy could be determined at the 95% CL, and the CP violating phase δ could be measured with a 95% CL error lower than 20°, if $\sin^2 2\theta_{13} > 0.01$ (i.e. $\theta_{13} > 3^\circ$) assuming the more conservative exposure scenario. All the sensitivities quoted here are computed assuming the 2 d.o.f statistical approach, and in our analysis we have included statistical and a 2% overall systematic error.

In summary, the *low energy neutrino factory* scenario could provide the ideal laboratory for precision lepton physics if the mixing angle $\theta_{13} > 2^\circ$.

Acknowledgments

We thank Stephen Parke for stimulating ideas. O. M. would like to thank D. Meloni for comments on the manuscript. This work was supported in part by the European Programme "The Quest for Unification" contract MRTN-CT-2004-

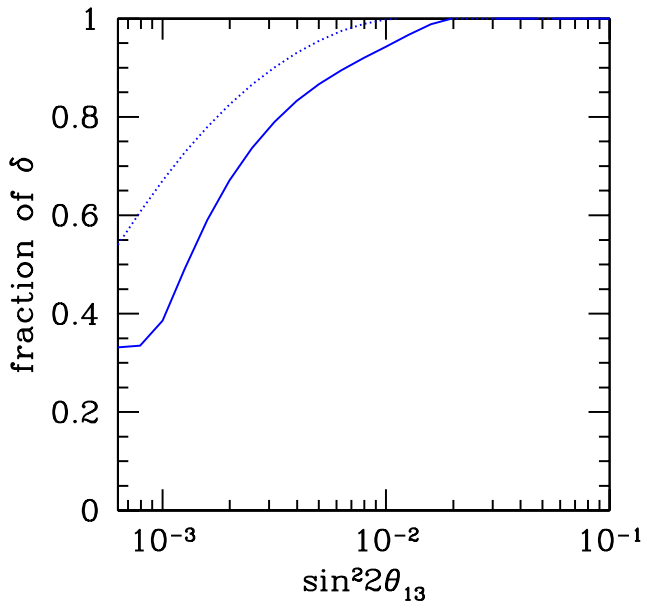

FIG. 7: 95% *CL hierarchy resolution (2 d.o.f) assuming that the far detector is located at a distance of* 1480 *km at the Henderson mine. The solid (dotted) curves depict the results assuming* 3×10^{22} *Kton-decays (*1×10^{23} *Kton-decays).*

503369, and by the Fermi National Accelerator Laboratory, which is operated by the Fermi Research Association, under contract No. DE-AC02-76CH03000 with the U.S. Department of Energy.

[1] B. T. Cleveland *et al.*, Astrophys. J. **496**, 505 (1998); Y. Fukuda *et al.* [Kamiokande Collaboration], Phys. Rev. Lett. **77**, 1683 (1996); J. N. Abdurashitov *et al.* [SAGE Collaboration], J. Exp. Theor. Phys. **95**, 181 (2002); W. Hampel *et al.* [GALLEX Collaboration], Phys. Lett. B **447**, 127 (1999); T. A. Kirsten [GNO Collaboration], Nucl. Phys. Proc. Suppl. **118**, 33 (2003).
[2] S. Fukuda *et al.* [Super-Kamiokande Collaboration], Phys. Lett. B **539**, 179 (2002).
[3] Q. R. Ahmad *et al.* [SNO Collaboration], Phys. Rev. Lett. **87**, 071301 (2001).
[4] Q. R. Ahmad *et al.* [SNO Collaboration], Phys. Rev. Lett. **89**, 011301 (2002) and *ibid.* **89**, 011302 (2002).
[5] S. N. Ahmed *et al.* [SNO Collaboration], Phys. Rev. Lett. **92**, 181301 (2004).
[6] B. Aharmim *et al.* [SNO Collaboration], Phys. Rev. C **72**, 055502 (2005).
[7] Y. Ashie *et al.* [Super-Kamiokande Collaboration], Phys. Rev. D **71**, 112005 (2005).
[8] K. Eguchi *et al.* [KamLAND Collaboration], Phys. Rev. Lett. **90**, 021802 (2003).
[9] M. H. Ahn [K2K Collaboration], hep-ex/0606032.
[10] A. Aguilar *et al.* [LSND Collaboration], Phys. Rev. D **64**, 112007 (2001).
[11] A. A. Aguilar-Arevalo *et al.* [MiniBooNE Collaboration], The MiniBooNE Run Plan, available at `http://www-boone.fnal.gov/publicpages/runplan.ps.gz`
[12] B. Pontecorvo, Sov. Phys. JETP **6**, 429 (1957) [Zh. Eksp. Teor. Fiz. **33**, 549 (1957)] and *ibid.* **7**, 172 (1958) [*ibid.* **34** (1958) 247]; Z. Maki, M. Nakagawa and S. Sakata, Prog. Theor. Phys. **28**, 870 (1962).
[13] M. Apollonio *et al.* [CHOOZ Collaboration], Phys. Lett. B **466**, 415 (1999).
[14] F. Boehm *et al.*, Phys. Rev. Lett. **84**, 3764 (2000); and Phys. Rev. D **62**, 072002 (2000).
[15] E. Ables *et al.* [MINOS Collaboration], FERMILAB-PROPOSAL-0875.
[16] D. G. Michael *et al.* [MINOS Collaboration], Phys. Rev. Lett. **97**, 191801 (2006).
[17] T. Schwetz, Phys. Scripta **T127**, 1 (2006).
[18] G. L. Fogli *et al.*, arXiv:hep-ph/0608060.
[19] T. Araki *et al.* [KamLAND Collaboration], Phys. Rev. Lett. **94**, 081801 (2005).
[20] S. Geer, Phys. Rev. D **57**, 6989 (1998) [Erratum-ibid. D **59**, 039903 (1999)].
[21] A. De Rujula, M. B. Gavela and P. Hernandez, Nucl. Phys. B **547**, 21 (1999).

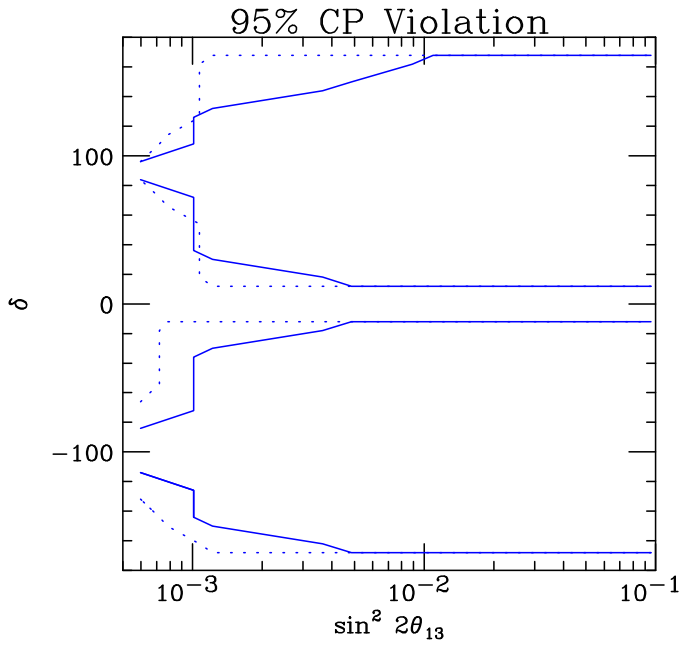

FIG. 8: 95% *CL CP Violation extraction (2 d.o.f) assuming that the far detector is located at a distance of* 1480 *km at the Henderson mine. The solid (dotted) curves depict the results assuming* 3×10^{22} *Kton-decays* (1×10^{23} *Kton-decays).*

[22] V. D. Barger, S. Geer and K. Whisnant,
[23] A. Donini *et al*, Nucl. Phys. B **574**, 23 (2000).
[24] V. D. Barger *et al*, Phys. Rev. D **62**, 013004 (2000).
[25] V. D. Barger *et al*, Phys. Rev. D **62**, 073002 (2000).
[26] A. Cervera, *et al* Nucl. Phys. B **579**, 17 (2000) [Erratum-ibid. B **593**, 731 (2001)].
[27] M. Freund, P. Huber and M. Lindner, Nucl. Phys. B **585**, 105 (2000).
[28] V. D. Barger *et al*, Phys. Lett. B **485**, 379 (2000).
[29] J. Burguet-Castell *et al*, Nucl. Phys. B **608**, 301 (2001).
[30] M. Freund, P. Huber and M. Lindner, Nucl. Phys. B **615**, 331 (2001).
[31] A. Donini, D. Meloni and P. Migliozzi, Nucl. Phys. B **646**, 321 (2002);
D. Autiero *et al.*, Eur. Phys. J. C **33**, 243 (2004).
[32] C. Albright *et al.*, arXiv:hep-ex/0008064;
[33] A. Blondel *et al.*, Nucl. Instrum. Meth. A **451**, 102 (2000);
M. Apollonio *et al.*, arXiv:hep-ph/0210192;
C. Albright *et al.* [Neutrino Factory/Muon Collider Collaboration], arXiv:physics/0411123.
[34] O. Mena, Mod. Phys. Lett. A **20**, 1 (2005).
[35] P. Huber, M. Lindner, M. Rolinec and W. Winter, hep-ph/0606119.
[36] P. Zucchelli, Phys. Lett. B **532**, 166 (2002).
[37] M. Mezzetto, J. Phys. G **29**, 1781 (2003) and *ibid.* **29** 1771 (2003).
[38] J. Burguet-Castell *et al.*, Nucl. Phys. B **695**, 217 (2004)
[39] A. Donini *et al.*, Nucl. Phys. B **710**, 402 (2005).
[40] J. Burguet-Castell *et al.*, Nucl. Phys. B **725**, 306 (2005).
[41] P. Huber *et al.*, hep-ph/0506237.
[42] A. Donini and E. Fernandez-Martinez, arXiv:hep-ph/0603261.
[43] A. Donini *et al.*, hep-ph/0604229.
[44] N. Holtkamp and D. Finley, eds., FERMILAB-PUB-00/108-E
[45] S. Ozaki *et al.*, BNL-52623,2001
[46] S. Geer and M. Zisman, eds., BNL-72369-2004, FERMILAB-TM-2259, LBNL-55478;
S. Geer and M.S. Zisman, FERMILAB-PUB-06-454-E, Submitted to Prog. Part. Nucl. Phys.
[47] D. Ayres *et al.*, Oscillations in the Fermilab NuMI Beamline," hep-ex/0503053.
[48] M. Ellis, "ISS Detector Working Group Report", presented at the 8th International Workshop on Neutrino Factories, Superbeams and Betabeams (NUFACT06), UC Irvine, August 24-30,2006, http://nufact06.physics.uci.edu/Default.aspx
[49] G. L. Fogli and E. Lisi, Phys. Rev. D **54**, 3667 (1996).
[50] H. Minakata and H. Nunokawa, JHEP **0110**, 001 (2001).
[51] V. D. Barger, S. Geer, R. Raja and K. Whisnant, Phys. Rev. D **63**, 113011 (2001).

[52] T. Kajita, H. Minakata and H. Nunokawa, Phys. Lett. B **528**, 245 (2002); H. Minakata, H. Nunokawa and S. J. Parke, Phys. Rev. D **66**, 093012 (2002); P. Huber, M. Lindner and W. Winter, Nucl. Phys. B **645**, 3 (2002); A. Donini, D. Meloni and S. Rigolin, JHEP **0406**, 011 (2004); M. Aoki, K. Hagiwara and N. Okamura, Phys. Lett. B **606**, 371 (2005); O. Yasuda, New J. Phys. **6**, 83 (2004); O. Mena and S. J. Parke, Phys. Rev. D **72**, 053003 (2005).
[53] H. Minakata and H. Nunokawa, Phys. Lett. B **413**, 369 (1997).
[54] V. Barger, D. Marfatia and K. Whisnant, Phys. Rev. D **66**, 053007 (2002).
[55] O. Mena Requejo, S. Palomares-Ruiz and S. Pascoli, Phys. Rev. D **72**, 053002 (2005).
[56] M. Ishitsuka *et al.*, Phys. Rev. D **72**, 033003 (2005); K. Hagiwara, N. Okamura and K. i. Senda, Phys. Lett. B **637**, 266 (2006).
[57] O. Mena, S. Palomares-Ruiz and S. Pascoli, Phys. Rev. D **73**, 073007 (2006).
[58] T. Kajita *et al*, arXiv:hep-ph/0609286.
[59] J. Burguet-Castell *et al.*, Nucl. Phys. B **646**, 301 (2002);
[60] P. Huber, M. Lindner and W. Winter, Nucl. Phys. B **654**, 3 (2003).
[61] H. Minakata, H. Nunokawa and S. J. Parke, Phys. Rev. D **68**, 013010 (2003).
[62] V. Barger, D. Marfatia and K. Whisnant, Phys. Lett. B **560**, 75 (2003).
[63] K. Whisnant, J. M. Yang and B. L. Young, Phys. Rev. D **67**, 013004 (2003); P. Huber *et al.*, Nucl. Phys. B **665**, 487 (2003); P. Huber *et al.*, Phys. Rev. D **70**, 073014 (2004); A. Donini, E. Fernández-Martínez and S. Rigolin, Phys. Lett. B **621**, 276 (2005).
[64] O. Mena and S. J. Parke, Phys. Rev. D **70**, 093011 (2004).
[65] P. Huber, M. Maltoni and T. Schwetz, Phys. Rev. D **71**, 053006 (2005).
[66] A. Blondel *et al.*, hep-ph/0606111.
[67] O. Mena, H. Nunokawa and S. J. Parke, hep-ph/0609011; O. Mena, hep-ph/0609031.
[68] A. Bueno, M. Campanelli and A. Rubbia, Nucl. Phys. B **589** 577 (2000).
[69] A. Donini *et al* Nucl. Phys. B **743**, 41 (2006).
[70] E. K. Akhmedov *et al.*, JHEP **0404** 078 (2004).